

The perturbation pressure, p' , can be represented as the sum of a hydrostatic pressure perturbation p'_h and a nonhydrostatic pressure perturbation p'_{nh} , that is,

$$p' = p'_h + p'_{nh}. \quad (2.122)$$

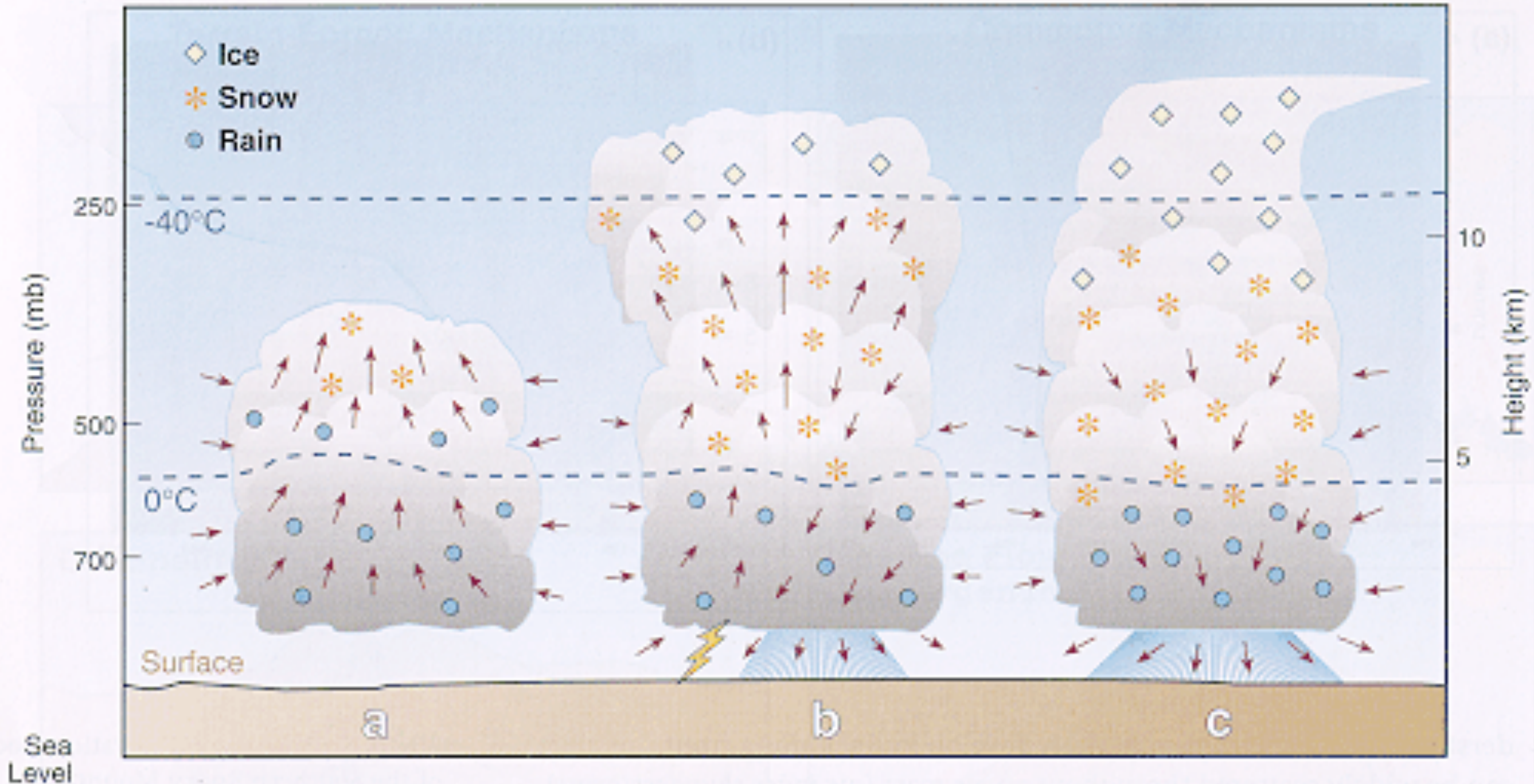
The former arises from density perturbations by way of the relation

$$\frac{\partial p'_h}{\partial z} = -\rho' g, \quad (2.123)$$

which allows us to rewrite the inviscid form of (2.56) as

$$\frac{dw}{dt} = -\frac{1}{\rho} \frac{\partial p'_{nh}}{\partial z}. \quad (2.124)$$

Hydrostatic pressure perturbations occur beneath buoyant updrafts (where $p'_h < 0$) and within the latently cooled precipitation regions of convective storms (where $p'_h > 0$) (e.g., Figure 5.23).



An

alternate breakdown of pressure perturbations is provided below.

$$\frac{dw}{dt} = -\frac{1}{\rho} \frac{\partial p'}{\partial z} - \frac{\rho'}{\rho} g \quad (2.75)$$

$$= -\frac{1}{\rho} \frac{\partial p'}{\partial z} + B \quad (2.76)$$

where $B (= -\frac{\rho'}{\rho} g)$ is the buoyancy and $-\frac{1}{\rho} \frac{\partial p'}{\partial z}$ is the vertical perturbation pressure gradient force. The vertical perturbation pressure gradient force arises from velocity gradients and density anomalies. A more thorough examination of

For well-behaved fields (i.e., $\nabla^2 p' \propto -p'$),

$$p' \propto \underbrace{\underbrace{e_{ij}^2}_{\text{splat}} - \frac{1}{2} |\boldsymbol{\omega}|^2}_{\text{dynamic pressure perturbation}} \underbrace{- \frac{\partial B}{\partial z}}_{\text{buoyancy pressure perturbation}} .$$

where

$$e_{ij}^2 = \frac{1}{4} \sum_{i=1}^3 \sum_{j=1}^3 \left(\frac{\partial u_i}{\partial x_j} + \frac{\partial u_j}{\partial x_i} \right)^2$$

and $u_1 = u$, $u_2 = v$, $u_3 = w$, $x_1 = x$, $x_2 = y$, and $x_3 = z$. Deformation describes the degree to which a fluid element changes shape as a result of spatial variations in the velocity field (e.g., fluid elements can be stretched or sheared by velocity gradients).

We see that deformation is always associated with high perturbation pressure via the e_{ij}^2 term, sometimes known as the *splat* term.¹¹ Rotation (of any sense) is always associated with low pressure by way of the $|\boldsymbol{\omega}|^2$ term, sometimes referred to as the *spin* term. We know that, hydrostatically, warming in a column leads to pressure falls in the region below the warming. The $\partial B/\partial z$ or *buoyancy pressure* term partly accounts for such hydrostatic effects.

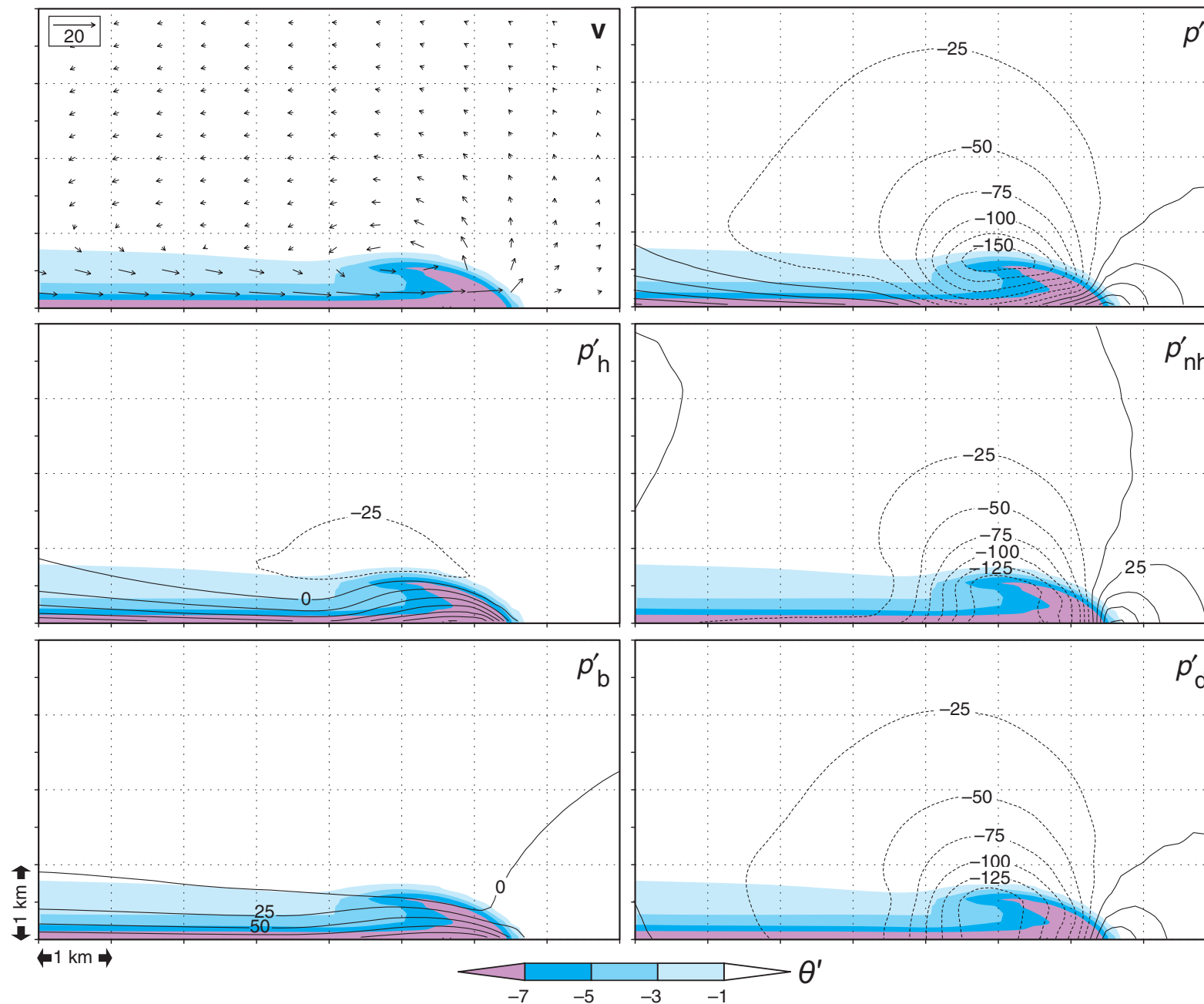
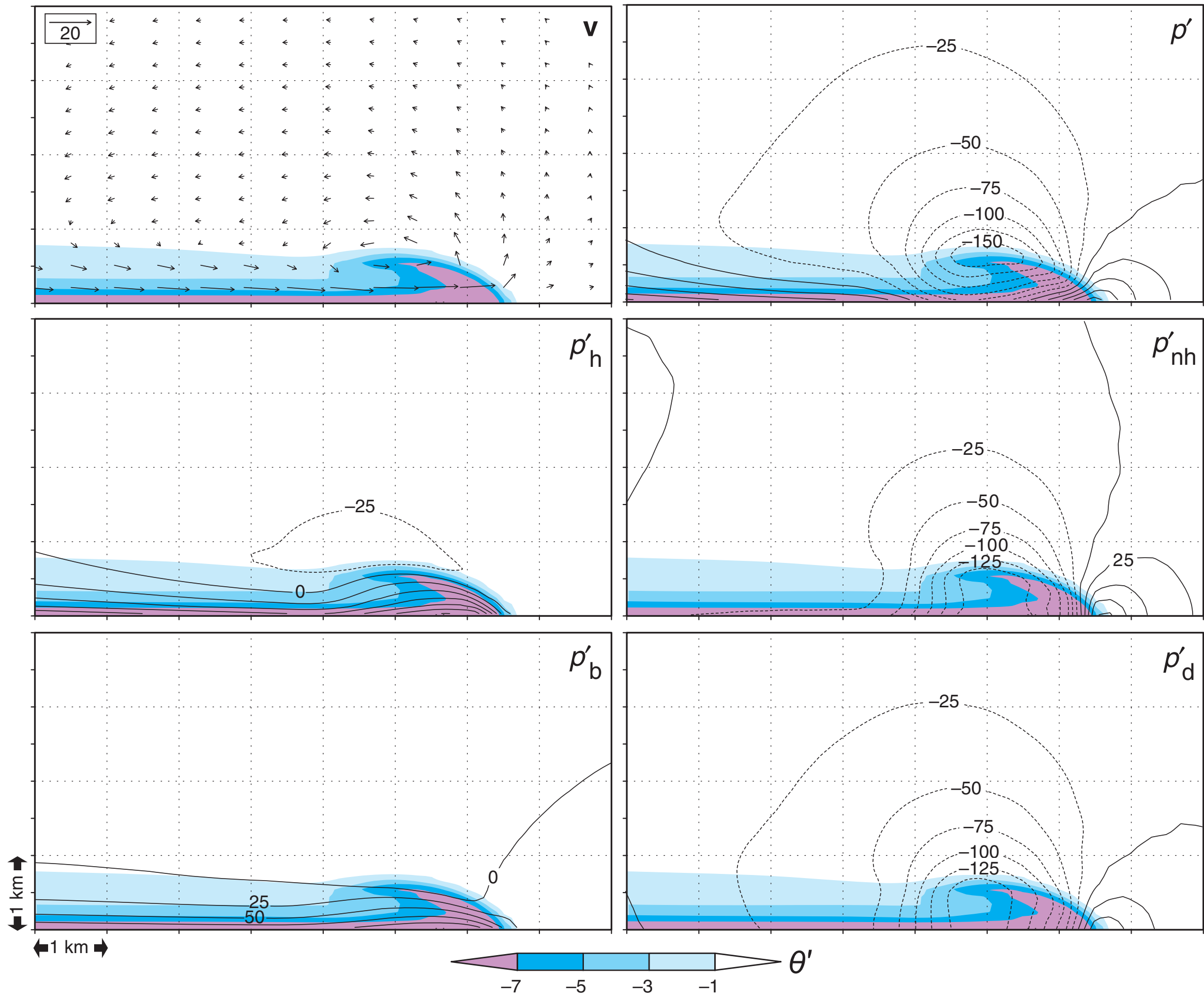


Figure 2.6 The pressure perturbations associated with a numerically simulated density current. The horizontal and vertical grid spacing of the simulation is 100 m. The ambient environment is unstratified. The domain shown is much smaller than the actual model domain used in the simulation. Potential temperature perturbations (θ') are shown in each panel (refer to the color scale). Wind velocity (\mathbf{v}) vectors in the x - z plane are shown in the top left panel (a reference vector is shown in the corner of this panel). Pressure perturbations are presented in the other panels. Units are Pa; the contour interval is 25 Pa = 0.25 mb (dashed contours are used for negative values). Note that $p' = p'_h + p'_{nh} = p'_d + p'_b$. The p'_b field was obtained by solving $\nabla^2 p'_b = \frac{\partial(\bar{\rho}B)}{\partial z}$, where $\bar{\rho}$ is the base state density, using periodic lateral boundary conditions and assuming $\frac{\partial p'_b}{\partial z} = 0$ at the top and bottom boundaries. (Regarding the boundary conditions, all that is known is that $\frac{\partial p'}{\partial z} = \bar{\rho}B$ at the top and bottom boundaries, owing to the fact that $dw/dt = 0$ at these boundaries, but it is somewhat arbitrary how one specifies the boundary conditions for $\frac{\partial p'_b}{\partial z}$ and $\frac{\partial p'_d}{\partial z}$ individually.) Because of the boundary conditions used, the retrieved p'_b field is not unique. A constant was added to the retrieved p'_b field so that the domain-averaged p'_b field is zero. The p'_d field was then obtained by subtracting p'_b from the total p' field.



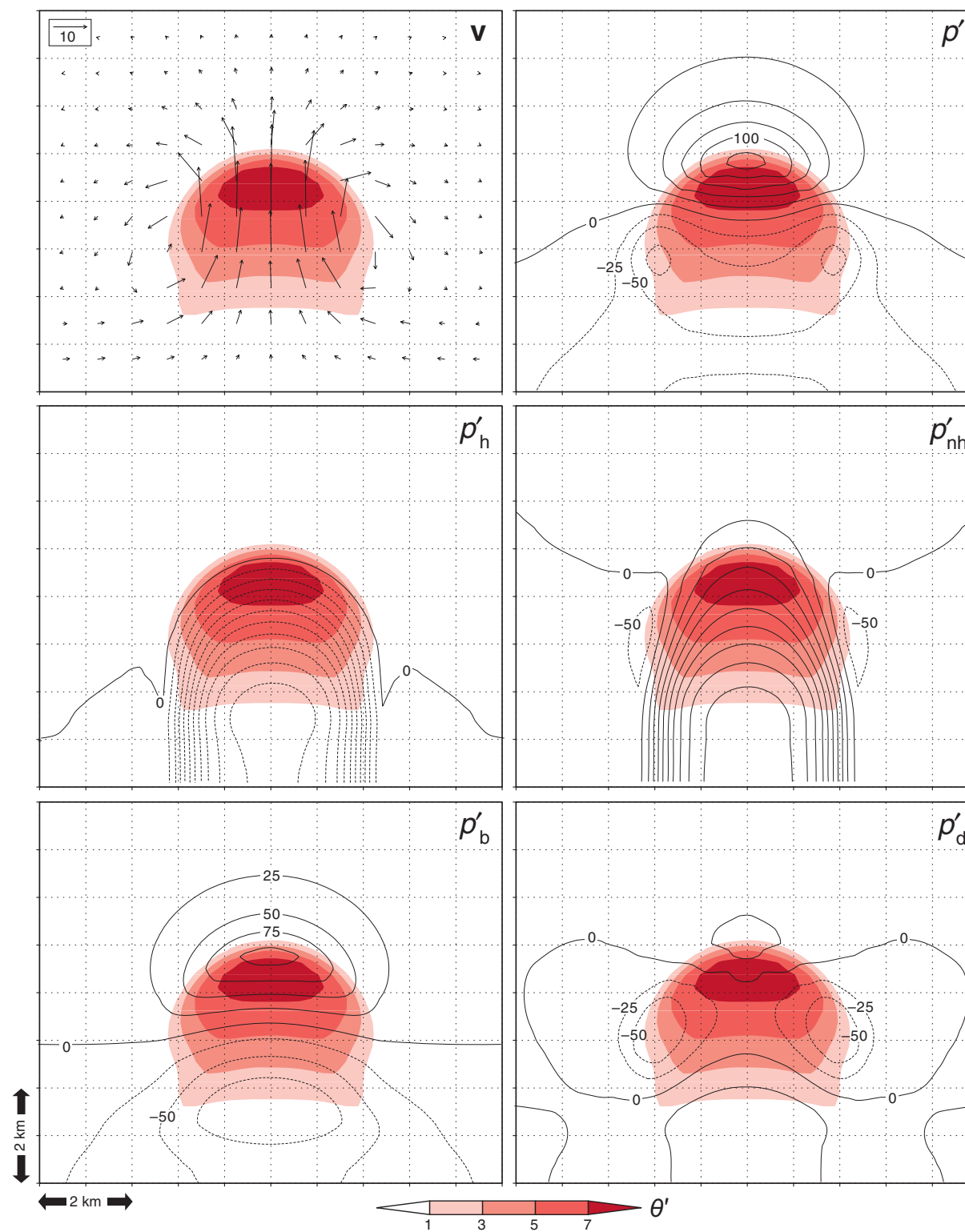
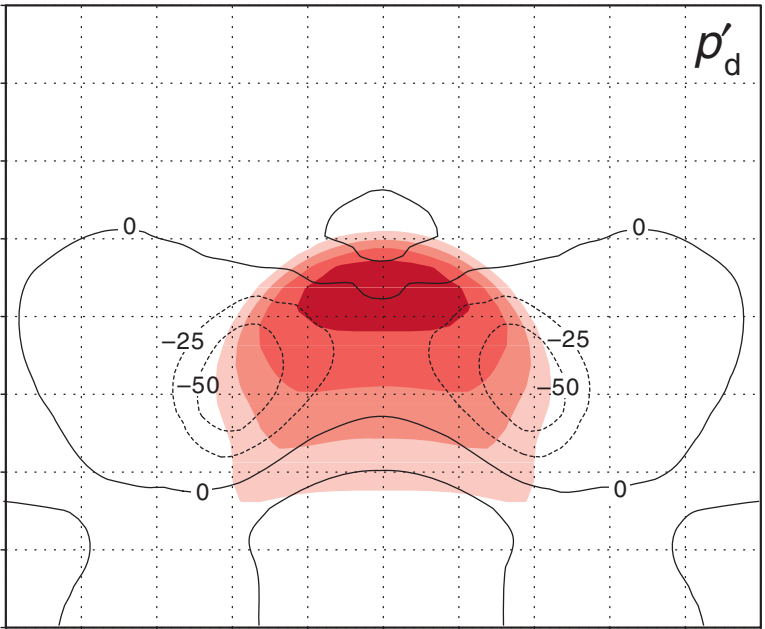
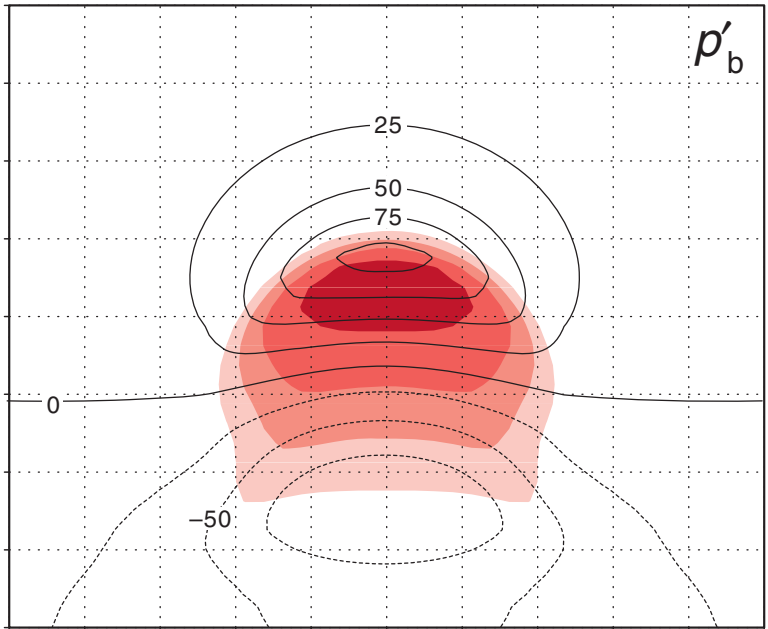
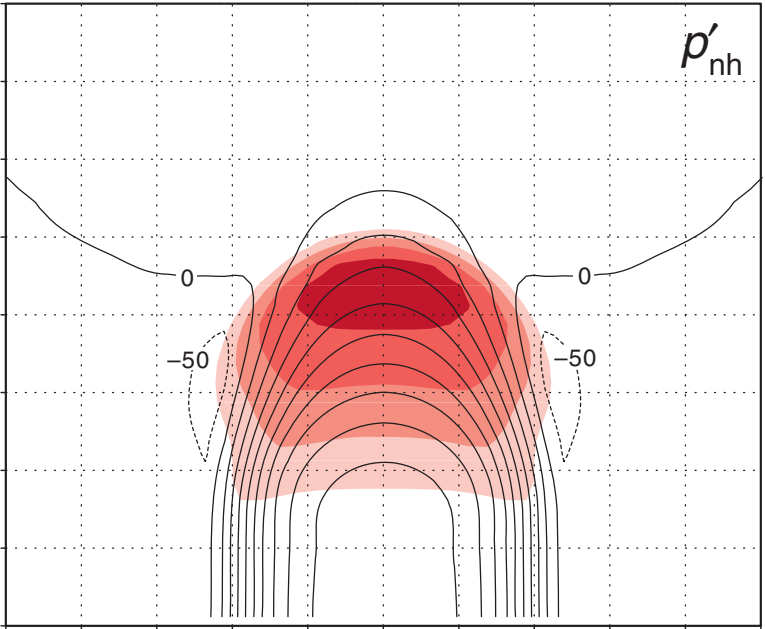
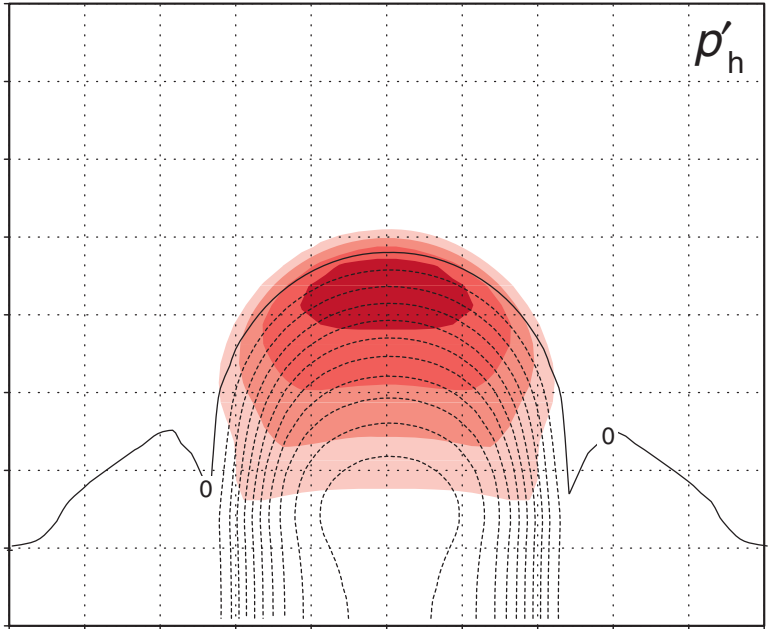
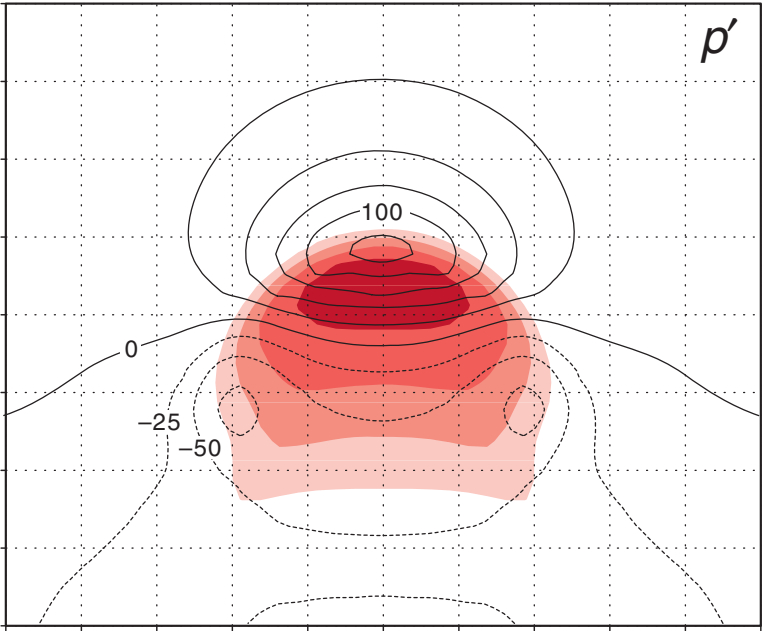
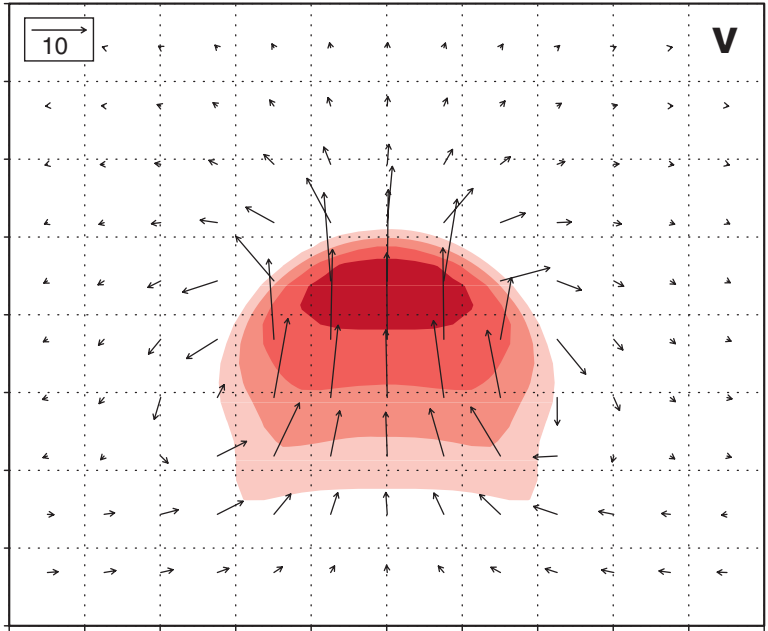
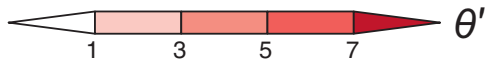


Figure 2.7 As in Figure 2.6, but for the case of a warm bubble released in a conditionally unstable environment. The bubble had an initial potential temperature perturbation of 2 K, a horizontal radius of 5 km, and a vertical radius of 1.5 km. The bubble was released 1.5 km above the ground. The fields shown above are from 600 s after the release of the bubble. The environment has approximately 2200 J kg^{-1} of CAPE and is the environment used in the simulations of Weisman and Klemm (1982). The horizontal and vertical grid spacing is 200 m (the domain shown above is much smaller than the actual model domain). The contour interval is 25 Pa (0.25 mb) for p' , p'_b , and p'_d . The contour interval is 50 Pa (0.50 mb) for p'_h and p'_{nh} .



2 km

2 km



3.1.1 *Vertical velocity of an updraft*

If we multiply both sides of (3.1) by $w \equiv dz/dt$, we obtain

$$w \frac{dw}{dt} = B \frac{dz}{dt} \quad (3.11)$$

$$\frac{d}{dt} \left(\frac{w^2}{2} \right) = B \frac{dz}{dt} \quad (3.12)$$

Next, we integrate (3.12) over the time required to travel from the LFC to the equilibrium level (EL). We assume $w = 0$ at the LFC, since the only force considered here is the buoyancy force, which, by definition, does not become positive until the LFC is reached. Also, we assume that the maximum vertical velocity, w_{\max} , occurs at the EL, which is consistent with the assumption that $dw/dt = B$ (neglecting the weight of hydrometeors in B).

Integration

of (3.12) yields

$$\int_{LFC}^{EL} dw^2 = 2 \int_{LFC}^{EL} B dz \quad (3.13)$$

$$w_{EL}^2 - w_{LFC}^2 = 2 \int_{LFC}^{EL} B dz \quad (3.14)$$

$$w_{\max}^2 = 2 \int_{LFC}^{EL} B dz \quad (3.15)$$

$$w_{\max} = \sqrt{2 \text{ CAPE}}. \quad (3.16)$$

$$w_{\max} = \sqrt{2 \text{ CAPE}}. \quad (3.16)$$

For $\text{CAPE} = 2000 \text{ J kg}^{-1}$, which corresponds to an average temperature (or virtual temperature) excess of $\approx 5 \text{ K}$ over a depth of 12 km, parcel theory predicts $w_{\max} = 63 \text{ m s}^{-1}$. The prediction of w_{\max} in a convective updraft by (3.16) typically is too large, for several reasons discussed in the next section. Therefore, the value of w_{\max} predicted by (3.16) can be interpreted as an upper limit for vertical velocity when buoyancy is the only force; w_{\max} sometimes is called the *thermodynamic speed limit*.⁴

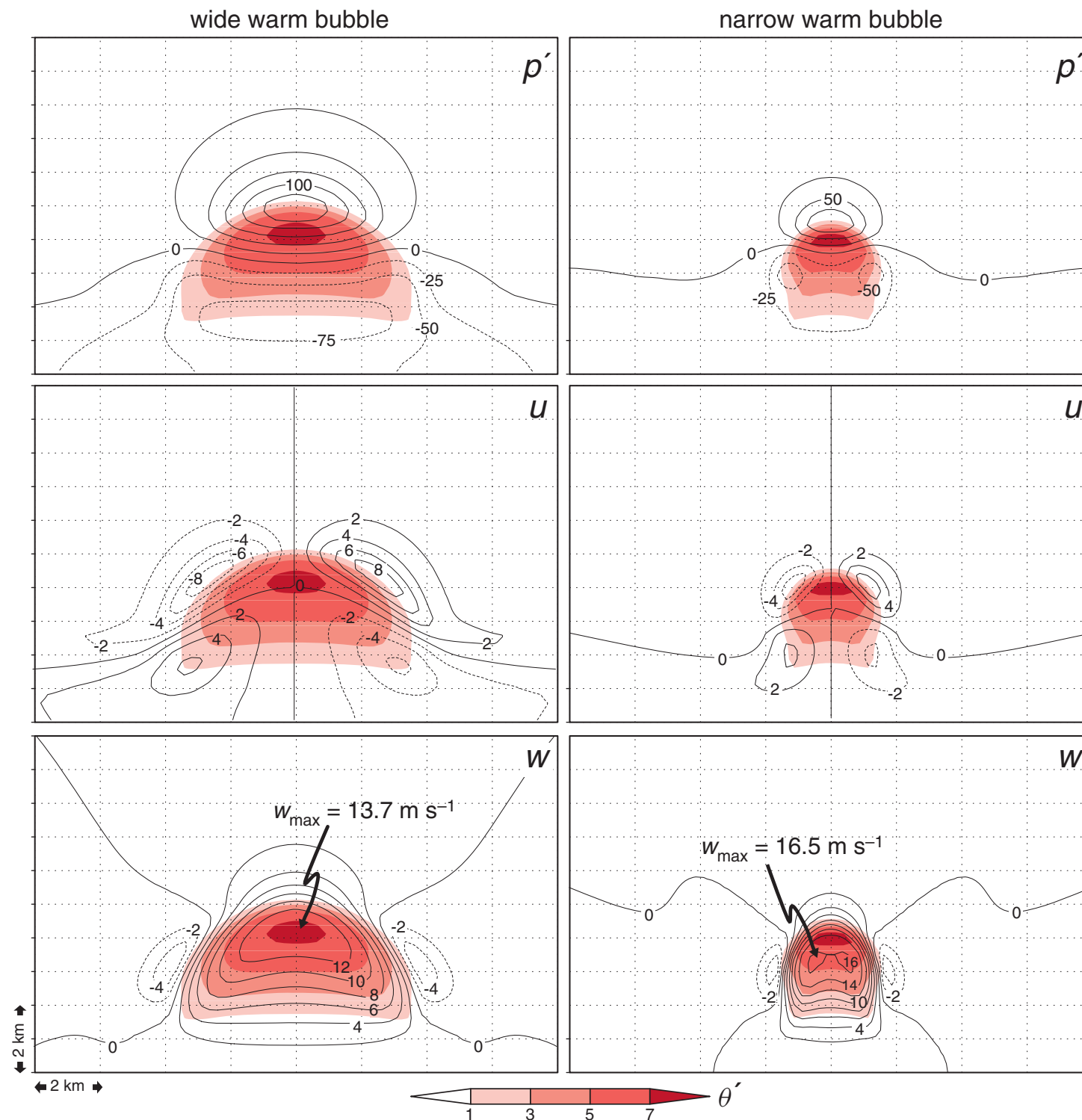


Figure 3.1 A comparison of the perturbation pressure (p') fields and zonal (u) and vertical (w) velocity components for the case of a wide warm bubble (left panels) and a narrow warm bubble (right panels) released in a conditionally unstable atmosphere in a three-dimensional numerical simulation. The contour intervals for p' and the wind components are 25 Pa and 2 m s^{-1} , respectively (dashed contours are used for negative values). Potential temperature perturbations (θ') are shown in each panel (refer to the color scale). The horizontal and vertical grid spacing is 200 m (the domain shown above is much smaller than the actual model domain). Both warm bubbles had an initial potential temperature perturbation of 2 K and a vertical radius of 1.5 km, and were released 1.5 km above the ground. The wide (narrow) bubble had a horizontal radius of 10 km (3 km). In the simulation of the wide (narrow) bubble, the fields are shown 800 s (480 s) after its release. The fields are shown at times when the maximum buoyancies are comparable. Despite the comparable buoyancies, the narrow updraft is 20% stronger owing to the weaker adverse vertical pressure gradient.

wide warm bubble

narrow warm bubble

